IUST
Iran University of Science and Technology

Iranian Journal of Electrical and Electronic Engineering

Journal Homepage: ijeee.iust.ac.ir

Research Paper

A New Fast and Accurate Fault Location and Classification Method on MTDC Microgrids Using Current Injection Technique, Traveling-Waves, Online Wavelet, and Mathematical Morphology

M. Dodangeh* and N. Ghaffarzadeh*(C.A.)

Abstract: In this paper, a new fast and accurate method for fault detection, location, and classification on multi-terminal DC (MTDC) distribution networks connected to renewable energy and energy storages presented. MTDC networks develop due to some issues such as DC resources and loads expanding, and try to the power quality increasing. It is important to recognize the fault type and location in order to continue service and prevent further damages. In this method, a circuit kit is connected to the network. Fault detection is performed with the measurement of the current of the connected kits and the traveling-waves of the derivative of the fault current and applying to a mathematical morphology filter, in the Fault time. The type and location of faults determinate using circuit equations and current calculations. DC series and ground arc faults are considered as DC distribution network disturbances. The presented method was tested in an MTDC network with many faults. The results illustrate the validity of the proposed method. The main advantages of the proposed fault location and classification strategy are higher accuracy and speed than conventional approaches. This method robustly operates to changing in sampling frequency, fault resistance, and works very well in high impedance fault.

Keywords: MTDC, Fault Detection and Classification, Mathematical Morphology, Current Injection Kit, Online Wavelet.

Nomenclature

R	Equivalent resistance of the kit and faulted part of the grid.
L	Equivalent inductance of the kit and faulted part of the grid.
C	Equivalent capacitance of the kit and faulted part of the grid.
i_p	Current of the faulted part of the grid.
d	Distance of fault location.
C_p, C_q	Capacitors of the kit.
S_b, S_p	switches of the kit.
L_p	Inductance of the kit.
V_b, R_b	Battery and resistance of the kit.
ω_n	The natural frequency.
α	The attenuation factor.
NG	Negative pole to ground fault.
PG	Positive pole to ground fault.
PN	Positive pole to negative pole fault.
f_d	Dilation of signals.
f_e	Erosion of signals.
f_c	The closing Function.
f_o	The opening Function.

Iranian Journal of Electrical and Electronic Engineering, 2020.
Paper first received 01 May 2019, revised 07 July 2019, and accepted 17 July 2019.
* The authors are with the Department of Electrical Engineering, Imam Khomeini International University, Qazvin 3414896818, Iran.
E-mails: mostafadodangeh@edu.ikiu.ac.ir and ghaffarzadeh@eng.ikiu.ac.ir.
Corresponding Author: N. Ghaffarzadeh.

1 Introduction

THE rapid and accurate detection and location of the fault are highly effective in improving the reliability indexes, increasing the speed of network repair, and reducing the recovery time and the expected energy not

supply. Increasing DC consumption in distribution networks, connecting DC renewable resources to the network, trying to increase the power quality and responding to further loads has expanded MTDC networks. And, the other hand, power electronic converters usage improves the size, weight, and equipment consumption and the load flow on the MTDC networks.

The implementation of conventional schemes for fault detection and location on MTDC networks has some problems. The accuracy of impedance-based methods is not sufficient at power frequency for distribution networks. Traditional protection methods that are based on under-voltage/over-current [1-6], rate of change in current/voltage [4] or either lack the required sensitivity for detecting high-resistance faults, or are Unreliable to communication delay and failure. Passive-Overcurrent protection based on discrete wavelet transform is proposed to different types of faults detection and classification [5]. Yet, none of the above schemes meet the speed requirement for an MTDC micro-grid [2], [5]. In [7], a directional current-based protection scheme is proposed for low voltage DC (LVDC) grids. However, apart from this schemes unreliability to communication failures, the operation of high bandwidth fiber optic communication is expensive and not justifiable for LVDC grids.

Traveling waves based methods have been used widely to detect transmission line faults [8-10]. Methods based on traveling waves and time domain analysis are used in HVDC networks [13]. In some methods, Wavelet has been mixed with other techniques such as fuzzy logic and artificial neural networks improve the performance of the proposed protection algorithm [8-17]. Some of these methods depend on the location of the fault and the arrival time of the traveling waves [19-20]. Determination of the fault location in the MTDC distribution grids should be done with high precision due to multiple and longitudinal branches. In [21-23], DC bus protection schemes in DC distribution networks have been suggested. The DC ring-bus protection techniques have been suggested [24-26]. The actual impedance approximation method is used in a network [27]. Detection of voltage drop in DC micro-grid is provided using the power probe unit proposed [28-31]. Few power electronics converter-based power probe units for injecting AC signals are used in [31-34]. In [35-37], transmission line protection method using mathematical morphology have been proposed. In this paper, a high-precision and high-speed method is proposed to fault location, detection, and classification in MTDC distribution networks using current injection, mathematical morphology, and online wavelet. Using the derivative of the traveling waves, online wavelet transform and mathematical morphology, the fault occurrence and its type and identified. The attenuation factor (α) is calculated based on the sampling of the derivative of the faults current in the network. This method was tested on an MTDC distribution network with many faults. The results illustrate the validation of the proposed method.

2 Method

2.1 Current Injection Technique

By adjoining the C_q branch to the current injection kit provided in [28], part of the switching current passing through this branch and reduces the switching losses and reduces the error of fault locating in the line close in fault. Fig. 1 illustrates the proposed kit. The current injection kit contains of tow capacitors an inductor, a battery and switches. The battery injects a current in the kit circuit through faulted path. The injected current will be small and remains for a period only. The C_p and L_p are the inductance and capacitance of the kit respectively. The C_p is equal to 27μF and the L_p is equal to 657μH in simulations. The optimum value of C_q is selected by considering the total loss of switching, the cost of capacitors installing, and reactive losses. The kit that be shown in Fig. 1 connected to the MTDC network buses. Fig. 2 illustrate the equivalent circuit of the faulted network and the kit in the fault time. If the fault does not occur, the current does not pass through the connected kits.

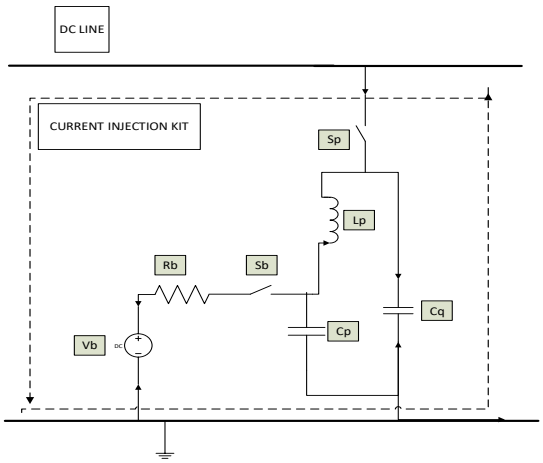

Fig. 1 Proposed current injection kit.

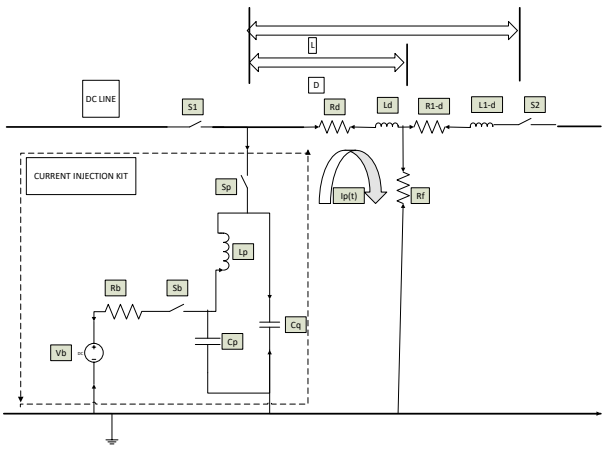

Fig. 2 Equivalent circuit of the faulted network and the kit.

The equation of the current of the faulted part of the grid is (1) and (2). The equivalent resistance and reluctance of the kit and faulted section of network are R and L.

$$\frac{d^2 i_p(t)}{dt^2}+\frac{R}{L}\frac{di_p(t)}{dt}+\frac{1}{LC}i_p(t)=0 \tag{1}$$

$$i_p(t)=K_1 e^{-\alpha t}\cos(\omega_d t)+K_2 e^{-\alpha t}\sin(\omega_d t) \tag{2}$$

where

$$\omega_d=\sqrt{\omega_n^2-\alpha^2}$$

$$\alpha=\frac{R}{2L}$$

$$\omega_n=\sqrt{\frac{L_d+C_q}{C_pC_q(L_d+L_p)+C_pL_dL_p}}$$

Due to the line impedance-to-length dependence, the natural frequency (ω_n) calculates by. (3).

$$\omega_n=\sqrt{\frac{L_u d+C_q}{C_pC_q(L_u d+L_p)+C_pL_u dL_p}} \tag{3}$$

Thus, the location of the fault occurrence is calculated using (4) and the error percent of the estimation of fault location is calculated by (5).

$$d=\frac{C_q-L_pC_pC_q\omega_n^2}{L_u\left(C_p(C_q+L_p)\omega_n^2-1\right)}=\frac{C_q-L_pC_pC_q(\omega_d^2+\alpha^2)}{L_u\left(C_p(C_q+L_p)(\omega_d^2+\alpha^2)-1\right)} \tag{4}$$

$$\epsilon=\left|\frac{d_{cal}-d_{act}}{d_{act}}\right|\times 100 \tag{5}$$

The equation of the curve of the fault current and its derivatives is (6), and by having two samples of the derivative of the fault current, the attenuation factor (α) is calculated by (7).

$$i_{pp}(t)=Ke^{-\alpha t} \tag{6}$$

$$\alpha_n=\frac{\ln(i'_n)-\ln(i'_{n+1})}{t_{n+1}-t_n} \tag{7}$$

2.2 Online Wavelet Transform

The wavelet transform keeps the relationship between the frequency and time of the signal and is a very good ability at the time-frequency resolution. This feature of the wavelet transform can be used to determine the arrival time of the traveling wave and its subsequent reflections. It is well known that discrete wavelet transform (DWT) is employed to various sampled (digitized) signals, to show their time-scale representation. In order to execute this transform, the original signal is passed into a band-pass filter (*G* is named mother wavelet) to give a detail component, for the first level. At the same level, and by convolving the signal with a low-pass filter (*H*), results in an approximate component. *G* and *H* are orthogonal vectors with *N*×1 elements [26]. For the second level, the approximate component is down-sampled by two, i.e. its samples are halved, and then are passed into *G* and *H* to give the next level approximate and detail components, respectively at this level. Continuing this method m to the *j*-th level, makes the original signal to be decomposed to *j* detail components and an approximate one. This scheme is presented in Fig. 3 up to four decomposition levels.

To show the above description in a mathematical form, for the *j*-th level of decomposition, the detail, and approximate components may be found as (8) and (9).

$$Aj=Aj-1\times G \tag{8}$$

$$Dj=Aj-1\times H \tag{9}$$

According to the aforementioned descriptions, in order to find the *j*-th level detail component, a serial process must be done through successive convolutions of approximate components with band-pass and low-pass filters up to the wanted decomposition level.

In on-line usages of DWT, this successive method, which is time-consuming, is not acceptable. In these applications, some detail or approximate components at some predefined frequency bands (various levels of decomposition) must be inspected. But, according to (8) and (9), the elements of the components in the *j*-th level cannot be computed unless the approximate component of the (j-1)th level is fully finished, and the latter cannot be defined unless the computations of the previous level are finalized. Consequently, the monitoring or inspecting mission cannot be produced, unless through a successive method. In this section, a digital filter for on-line applications of DWT is formed. The first feature of this filter is that the *k*-th element of *D*1 or *A*1 comes out along with the kth element of all of the upper-level detail or approximate components. Let (1) and (2) with *j*=2 to be rewritten as (10) and (11):

$$A2=A1\times G=X\times G\times G \tag{10}$$

$$D2=A1\times H=X\times G\times H \tag{11}$$

Therefore

$$Gj=HjjGj-1=\left(\prod_{(m=2)}^{j}Hmm\right)G \tag{12}$$

$$Aj=X\times Gj \tag{13}$$

$$Dj=X\times Gj \tag{14}$$

In the same way, the matrix for generating the elements of online approximate components can be

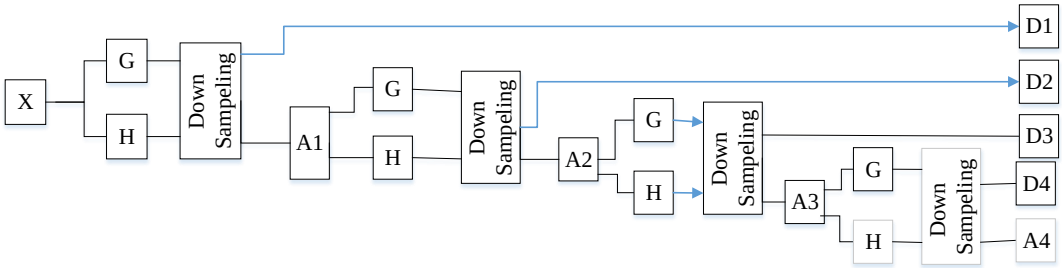

Fig. 3 Four decomposition levels of main signal X by DWT.

introduced [39].

2.3 Mathematical Morphology Filter

Mathematical morphology is a non-linear analyzing Technique of signal with low computational complexity and high accuracy that can be used to extract information from high-frequency signals. Mathematical morphology in the field of time and with brief information windows examines the appearance of high-frequency signals. The dilation and erosion of the input signal (F) with the domain D_f and the structural element (G) with the domain D_g are defined as (15) and (16). And using the dilation and erosion the open and close relations are defined as (17) and (18), and the morphological filter is defined according to the four relations that have been introduced in the form of (19).

$$f_d(n)=(f\oplus g)(n)=\max\{f(n-m)+g(m)\} \quad (15)$$

$$f_e(n)=(f\ominus g)(n)=\max\{f(n+m)-g(m)\} \quad (16)$$

$$f_o(n)=(f\circ g)(n)=((f\oplus g)\ominus g)(n) \quad (17)$$

$$f_c(n)=(f\bullet g)(n)=((f\ominus g)\oplus g)(n) \quad (18)$$

$$MF(n)=(f(n)\circ(f\bullet g)(n)+f(n)\bullet(f\circ g)(n))/2 \quad (19)$$

Such that

$$n\in D_f \text{ and } m\in D_g$$

$$D_f=\{0,1,2,\ldots,N-1\}$$

$$D_g=\{0,1,2,\ldots,M-1\}$$

Equation (19) filter operates at high accuracy in detecting the range of disturbances but is incapable of detecting the direction of the disturbance signal. This problem is resolved by using (20).

$$MMF(n)=\begin{cases}MF_d(n)-MF_e(n), & MF_d(n)>MF_d(n-1)\\ MF_e(n)-MF_d(n), & MF_e(n)>MF_e(n-1)\end{cases} \quad (20)$$

Based on [32-34], when the erosion signal lags the dilation signal, the MMF output has a positive pole; when the erosion signal leads the dilation signal, the MMF output has a negative pole. Also, when there is no sudden change in the initial signal, there is not the phase difference between the erosion and dilation signals and the MMF output is zero.

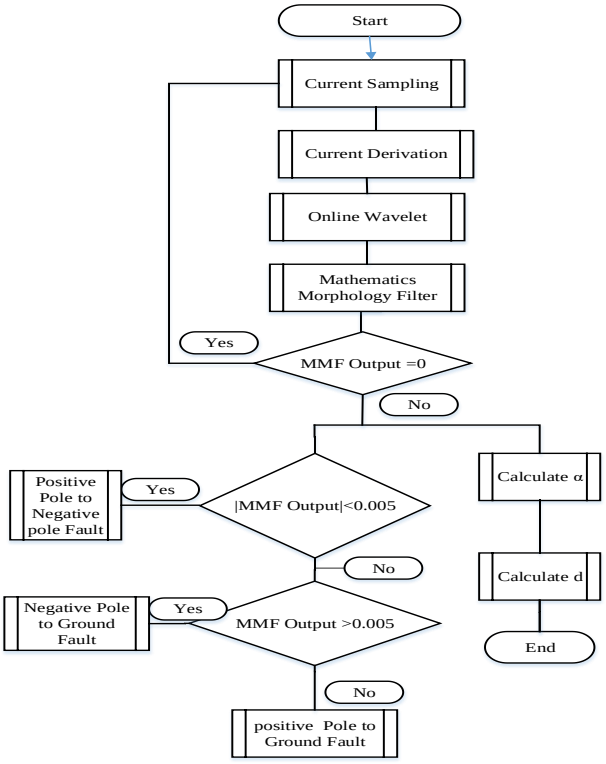

Fig. 4 Proposed method flowchart.

With applying the online wavelet to the derivative of the disturbance signal in MTDC distribution networks, traveling waves is obtained.

The traveling wave of the derivative of the disturbance signal, for various types of fault, applied to the morphological filter and faults type is detected. Many types of faults are simulated in the Cigre benchmark MTDC network and the accuracy of the proposed method is validated in part 3. The proposed method's Flowchart is shown in Fig. 4. This algorithm is divided into 3 part and 8 steps as follows:

Fault detection steps:

Step 1: Measuring and digitalize the current.

Step 2: Calculate the fault current derivative.

Step 3: Calculate traveling waves of fault current derivative using online-wavelet.

Step 4: Calculate the output of mathematical morphology filter.

Step 5: If MMF=0 then go to step 1 else go to fault

location and fault classification steps.

Fault classification step:

Step 6: If |MMF|<0.005 the positive pole to negative pole fault occurred.

Else if MMF>0.005 the negative pole to ground fault occurred.

Else the positive pole to ground fault occurred.

Fault location steps:

Step 7: Calculate the attenuation factor (α) by (7).

Step 8: Calculate the fault location by (5).

3 Simulation Result

In order to examine the proposed method, a multi-terminal DC distribution network was simulated in PSCAD/EMTDC software. This network includes cable and overhead lines and connected to the power grid and several distributed generation and energy storage. Distributed generation include wind energy, photovoltaic and diesel generator. Fig. 5 illustrates this network. Different types of faults were simulated with different conditions in terms of the location of faults, arc's resistance, and type of faults.

Fault current signals were measured in all mode. The sampling frequency is 2kHz. In each case, two samples method used to calculate the fault current derivative. Using the MATLAB software's wavelet toolbox traveling waves was calculated from fault current derivative. By applying the resulted waves to the mathematical morphology filter the type of faults was determined for different situations with high precision. Determine the fault location in each case using (4) and the fault location error percent calculated in each case by (5). Results of some of the simulations are presented in Table 1.

Three types of faults were applied, with the distance of 40% of the length of the line between the bus Bb-E1 and the bus Bb-D1 and among the fault's resistance equal to 25Ω, including positive pole to the ground, negative pole to the ground and positive pole to negative pole. Fault currents were measured in three modes. Fig. 6(a) shows the fault currents in each type of operated fault.

The three-mode wavelets of fault currents' derivative were calculated, using online wavelet and db4 as mother wavelet. Using online wavelet has increased the speed of fault detection and fault classification. Fig. 6(b) illustrates its diagrams.

Fig. 6(c) shows the output of the mathematical morphology filter for three types of faults. Depending on the diagrams of Fig. 6(c), the proposed method operates with high accuracy and speed to detect types of faults. The fault type is detect before fifth sample in pole to ground faults and in pole to pole faults indicate by eighth sample measuring. The proposed fault location technique works by three sample of disturbance signal.

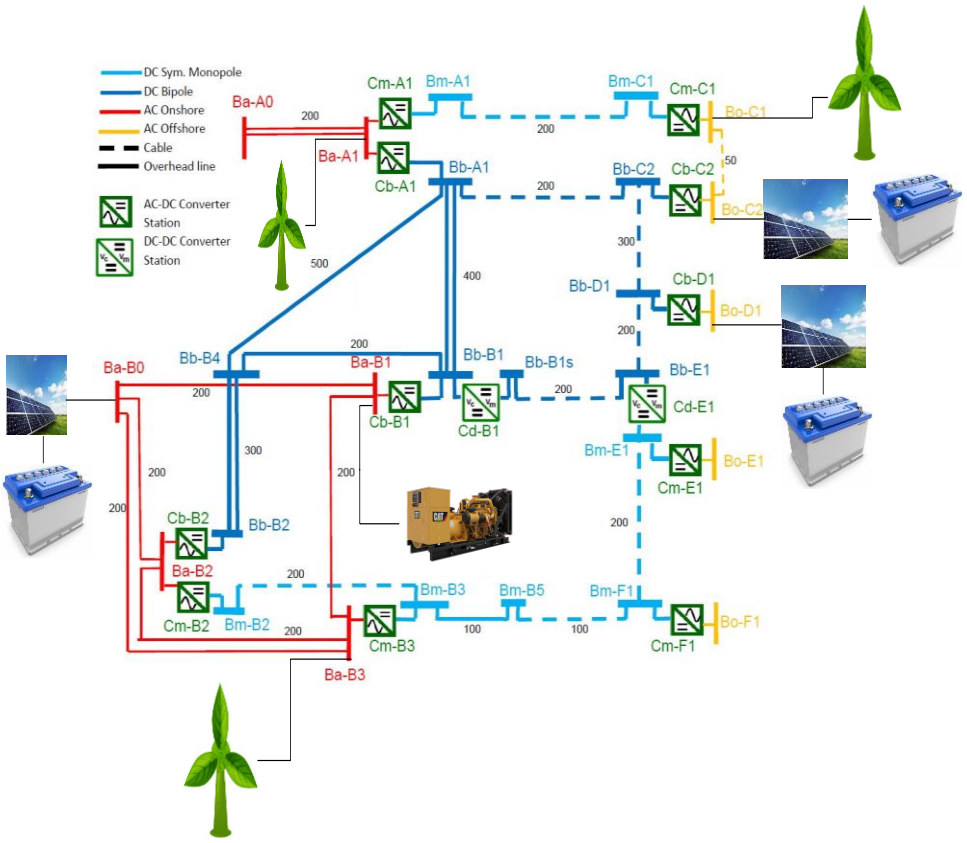

Fig. 4 Multi terminal direct current test network.

Table 1 Fault location and classification method's results.

	Fault			Fault resistance	Positive pole to the ground (PG) fault			Negative pole to the ground (NG) fault			Positive pole to negative pole (PN) fault		
	Beginning of Line	End of line	Actual fault distance [%]		Calculated fault distance [%]	Fault location error [%]	Fault type	Calculated fault distance [%]	Fault location error [%]	Fault type	Calculated fault distance [%]	Fault location error [%]	Fault type
1	Bb-B4	Bb-B1	5	0.05	4.9998	0.004	PG	4.99977	0.0046	NG	4.99984	0.0032	PN
2	Bb-E1	Bb-B1s	5	0.05	4.9997	0.006	PG	4.99981	0.0038	NG	4.99978	0.0044	PN
3	Bb-B4	Bb-B1	15	0.05	14.9998	0.001333	PG	15	0	NG	14.99977	0.001533	PN
4	Bb-B4	Bb-A1	30	0.05	30.0022	0.007333	PG	30	0	NG	30.0019	0.006333	PN
5	Bm-B5	Bm-F1	25	0.05	24.9989	0.0044	PG	25.0019	0.0076	NG	24.9991	0.0036	PN
6	Bb-A1	Bb-C2	45	0.05	44.9986	0.003111	PG	44.9979	0.004667	NG	45	0	PN
7	Bb-B4	Bb-A1	60	5	60	0	PG	60.0009	0.0015	NG	59.9992	0.001333	PN
8	Bb-B4	Bb-B2	40	5	40.0031	0.00775	PG	40.0007	0.00175	NG	39.9986	0.0035	PN
9	Bb-B1	Bb-A1	85	5	85.0029	0.003412	PG	85.002	0.002353	NG	85.0018	0.002118	PN
10	Bb-E1	Bb-B1s	5	50	5	0	PG	5.00023	0.0046	NG	5.00018	0.0036	PN
11	Bb-B4	Bb-B1	5	50	5.0002	0.004	PG	5.003	0.06	NG	5.0015	0.03	PN
12	Bm-E1	Bm-F1	15	50	15.0005	0.003333	PG	15.0011	0.007333	NG	15.00031	0.002067	PN
13	Bb-B1	Bb-A1	30	50	30.0004	0.001333	PG	30.0021	0.007	NG	30.0013	0.004333	PN
14	Bm-B3	Bm-B2	99	0.05	99	0	PG	98.999	0.0010101	NG	99.0008	0.000808	PN
15	Bb-B1	Bb-A1	45	0.05	44.998	0.004444	PG	44.9989	0.002444	NG	45	0	PN
16	Bm-B3	Bm-B5	55	0.05	55.0022	0.004	PG	54.99907	0.001691	NG	55.0031	0.005636	PN
17	Bb-E1	Bb-D1	40	0.05	40	0	PG	39.9989	0.00275	NG	40	0	PN
18	Bm-C1	Bm-A1	80	0.05	80.004	0.005	PG	80	0	NG	80	0	PN
19	Bb-C2	Bb-D1	50	5	50.0011	0.0022	PG	50.003	0.006	NG	50.0023	0.0046	PN
20	Bm-E1	Bm-F1	5	5	70	0	PG	70.00322	0.0046	NG	69.9989	1299.978	PN
21	Bb-E1	Bb-D1	10	5	10.0009	0.009	PG	10	0	NG	10	0	PN
22	Bm-B3	Bm-B5	95	50	95.0005	0.000526	PG	95.00064	0.0006736	NG	95	0	PN
23	Bm-B3	Bm-B2	65	50	65.0031	0.004769	PG	65.0047	0.007231	NG	65.0027	0.004154	PN
24	Bm-C1	Bm-A1	5	50	5.0001	0.002	PG	5.00041	0.0082	NG	5.000099	0.00198	PN
25	Bb-C2	Bb-D1	10	50	10.00071	0.0071	PG	10.00031	0.0031	NG	10.00062	0.0062	PN
26	Bm-E1	Bm-F1	35	50	35	0	PG	35.0018	0.005143	NG	35.002	0.005714	PN

4 Classification Criteria Selection

One thousand five hundred various faults were evaluated on the MTDC network with different conditions of arc resistance, sampling frequency, location and type of faults. Some of which are presented in Tables 1 and 2. The value of the mathematical morphology filter output of all case is given in Fig. 7. The fault classification criterion was considered equal to ±0.005 according to various simulations. Faults classify properly with selected thresholds according to Fig. 7.

5 Effect of the Fault Resistance on the Proposed Fault Location Method

By adding the C_q branch to the flow injection kit presented in [28] and installing the kits, the proposed fault location method was used to determine the fault location. Also, the error of the fault location was significantly reduced compared to the presented method in [28] for faults near the beginning of the line (close in fault) with high fault resistance. The error of the method presented in [28] is shown in Fig. 8. By applying different faults along the line and with variable values of arc resistance from zero to 100Ω using the proposed method, the location of the occurrence for all types of fault is calculated. Fig. 9 illustrate the average error of the three types of fault by the proposed fault location method.

According to Fig. 9 and the results of Table 1, the proposed method has a good response to the impedance fault. Faults with 100Ω resistance applied at various points along the line length and the fault location calculated using the proposed method. The average error of fault location is less than 2%. According to the above mentioned, this method is robust to high impedance fault.

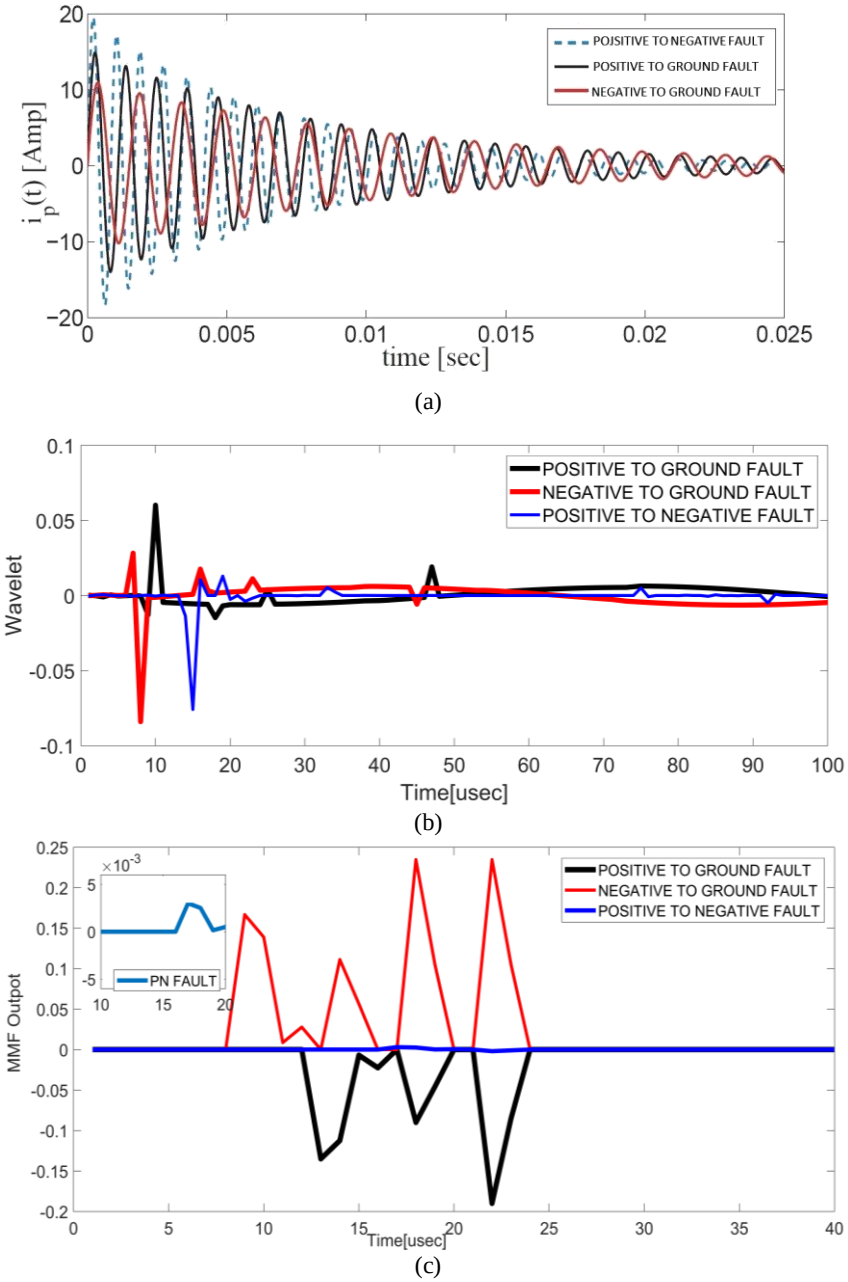

Fig. 6 a) Fault current in three mode, b) online wavelet output of fault current, and c) mathematical morphology filter output.

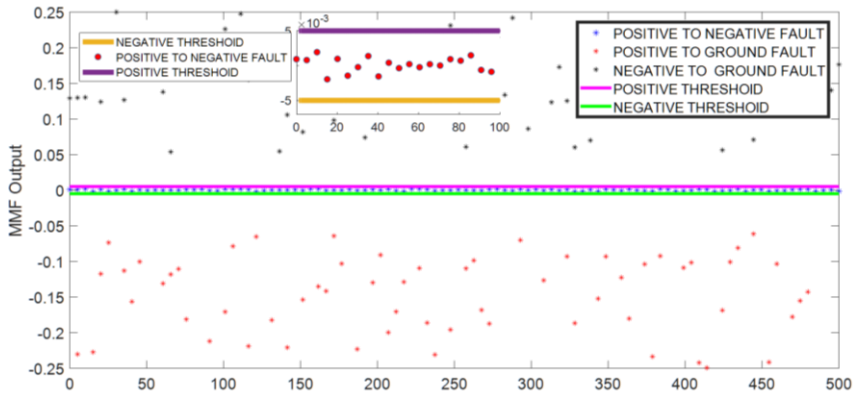

Fig. 7 Value of the mathematical morphology filter output of various faults.

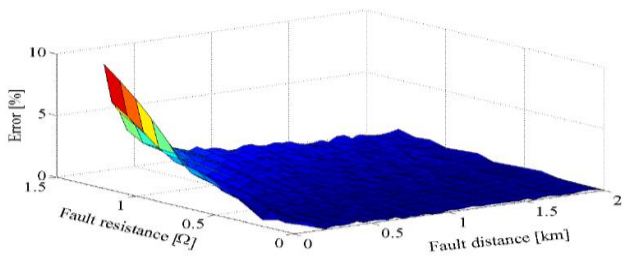

Fig. 8 Error of the method presented in [28].

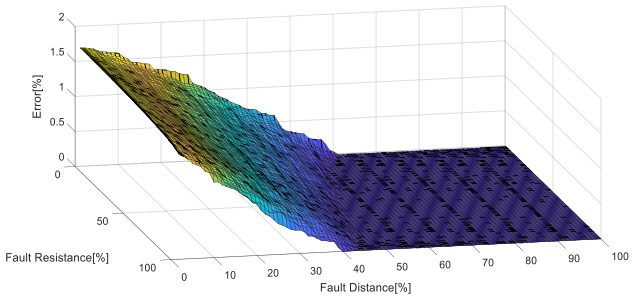

Fig. 9 Error of the presented method.

Table 2 Results of fault location method with various sampling frequency.

Sampling frequency [kHz]	Actual fault distance [%]	5	5	25	30	45	60	85	95
	Fault resistance	0.05	50	0.05	50	5	50	0.05	5
0.5	Estimated fault distance [%]	4.9996	4.999	25.02	30.0019	44.97	60.1	84.94	95.54
	Fault location error [%]	0.008	0.02	0.08	0.00634	0.06667	0.1667	0.0706	0.4632
1	Estimated fault distance [%]	5	5.001	24.99	30.0057	45.04	60.03	85.18	94.93
	Fault location error [%]	0	0.02	0.04	0.01899	0.08889	0.05	0.2118	0.0737
2	Estimated fault distance [%]	4.999	4.9994	25.1236	30.003	44.986	60	85.058	94.71
	Fault location error [%]	0.02	0.012	0.4944	0.01	0.0311	0	0.0683	0.3053
5	Estimated fault distance [%]	5.0037	5	25.003	30	44.972	60.156	85.08	95
	Fault location error [%]	0.074	0	0.012	0	0.06223	0.26	0.09412	0
10	Estimated fault distance [%]	5	5.005	24.994	29.99	45	59.8	84.96	95.19
	Fault location error [%]	0	0.01	0.024	0.03334	0	0.3334	0.04706	0.2
20	Estimated fault distance [%]	4.992	5.007	24.9926	29.993	44.979	60	84.9	94.54
	Fault location error [%]	0.16	0.14	0.0296	0.02334	0.04667	0	0.1176	0.4842
30	Estimated fault distance [%]	4.9995	5.0008	25.06	30.1	45.1	59.69	85.2	95
	Fault location error [%]	0.01	0.016	0.024	0.3334	0.22223	0.5167	0.2352	0
40	Estimated fault distance [%]	5.006	4.9991	25.009	29.989	45	60.08	85.09	94.62
	Fault location error [%]	0.12	0.018	0.036	0.03667	0	0.1334	0.1588	0.3948
50	Estimated fault distance [%]	4.999	5.009	25.019	30.015	45	60.07	84.96	95.08
	Fault location error [%]	0.02	0.018	0.076	0.05	0	0.1167	0.0047	0.0842

6 Sampling Frequency Effect

The proposed method was used for various faults by varying the sampling frequency from 500Hz to 50kHz, and the results of 0.5, 1, 2, 10, 20, 30, 40, and 50 kHz sampling frequencies are given in Table 2.

The results of Table 2 clearly show that changing the sampling frequency in a widely range does not change the efficiency and accuracy of the proposed method in the fault locating. For each fault types using the proposed method, the fault location was calculated with very lowly error.

7 Conclusion

In this paper, a new method of fault detection and fault location in MTDC networks proposed which can be used to detect and classify faults quickly, accurately and efficiently in MTDC networks. The location of the occurred fault is determine exactly by connecting a circuit kit to the network. Using the proposed kit reduces the error of the fault location, especially the faults occurred at the beginning of the line and near the kit. In fault occurrence, fault detection is done with measurement of traveling waves of fault current derivative by online wavelet and applying to a mathematical morphology filter. The fault type classification is done according to the mathematical filter morphology output. The fault location determine using the circuit equations and current calculations. The accuracy of the presented method in an MTDC system was examined with various faults in terms of type, location, resistance, and sampling frequencies. The proposed approach is robust to sampling frequency change and Arc resistance variations. The proposed method works with excellent performance in high impedance faults. More important, the proposed approach operates properly for any MTDC network, regardless of system's topology, that is, the number of network's radial lines, meshes, nodes, and rings.

Appendix

	Lines data		
	Resistance	Inductance	Voltage
Overhead line	120 mΩ/km	0.23 mH/km	380 V
Cable	100 mΩ/km	0.15 mH/km	380 V
	Sources data		
	Nominal power	Voltage	
Wind	25 kW	2.5 kV	
Photovoltaic	5 kW	0.6 kV	
Diesel generator	3 kVA	0.8 kV	
Battery	4 kW	0.6 kV	
AC grid	50 kVA	11 kV	
	Transformers data		
	Nominal power	HV side Voltage	LV side Voltage
Between wind and micro-grid converter	25 kVA	2.5 kV	380 V
Between AC grid and micro-grid converter	60 kVA	11 kV	380 V
Between photovoltaic and micro-grid converter	8 kVA		380 V

References

[1] A. Hooshyar and R. Iravani, "Microgrid protection," in *Proceedings of the IEEE*, Vol. 105, No. 7, pp. 1332–1353, Jul. 2017.

[2] N. Chaudhuri, B. Chaudhuri, R. Majumder, and A. Yazdani, *Multiterminal direct-current grids: Modeling, analysis, and control*. John Wiley & Sons, 2014.

[3] C. H. Noh, C. H. Kim, G. H. Gwon, and Y. S. Oh, "Development of fault section identification technique for low voltage DC distribution systems by using capacitive discharge current," *Journal of Modern Power Systems and Clean Energy*, Vol. 6, No. 3, pp. 509–520, Jun. 2018.

[4] S. D. A. Fletcher, P. J. Norman, S. J. Galloway, P. Crolla, and G. M. Burt, "Efficient protection scheme for low-voltage DC micro-grid," *IET Generation, Transmission & Distribution*, Vol. 12, No. 13, pp. 3322–3329, Jul. 2018.

[5] K. A. Saleh, A. Hooshyar, and E. F. El-Saadany, "Hybrid passive overcurrent relay for detection of faults in low-voltage DC grids," I*EEE Transactions on Smart Grid*, Vol. 8, No. 3, pp. 1129–1138, May 2017.

[6] M. E. Baran and N. R. Mahajan, "Overcurrent protection on voltage source- converter-based multiterminal DC distribution systems," *IEEE Transactions on Power Delivery*, Vol. 22, No. 1, pp. 406–412, Jan. 2007.

[7] A. A. S. Emhemed, K. Fong, S. Fletcher, and G. Burt, "Validation of fast and selective protection scheme for an LVDC distribution network," *IEEE Transactions on Power Delivery*, Vol. 32, No. 3, pp. 1432–1440, Jun. 2017.

[8] S. Hasheminejad, S. G. Seifossadat, M. Razaz, and M. Joorabian, "Traveling-wave-based protection of parallel transmission lines using Teager energy operator and fuzzy systems," *IET Generation, Transmission & Distribution*, Vol. 10, No. 4, pp. 1067–1074, 2016.

[9] A. Abdollahi and S. Seyedtabaii, "Transmission line fault location estimation by Fourier & wavelet transforms using ANN," in *IEEE 4th International Power Engineering and Optimization Conference (PEOCO)*, pp. 573–578, Jan. 2010.

[10] S. N. Ananthan, R. Padmanabhan, R. Meyur, B. Mallikarjuna, M. J. B. Reddy, and D. K. Mohanta, "Real-time fault analysis of transmission lines using wavelet multi-resolution analysis based frequency domain approach," *IET Science, Measurement & Technology*, Vol. 10, No. 7, pp. 693–703, 2016.

[11] A. Yadav and A. Swetapadma, "Enhancing the performance of transmission line directional relaying, fault classification and fault location schemes using fuzzy inference system," *IET Generation, Transmission & Distribution*, Vol. 9, No. 6, pp. 580–591, 2015.

[12] J. M. Johnson and A. Yadav, "A complete protection scheme for fault detection, classification and location estimation in HVDC transmission lines using support vector machine," *IET Science, Measurement & Technology*, Vol. 11, No. 3, pp. 279–287, 2017.

[13] A. Rafinia and J. Moshtagh, "A new approach to fault location in three-phase underground distribution system using combination of wavelet analysis with ANN and FLS," *International Journal of Electrical Power & Energy Systems*, Vol. 55, pp. 261–274, 2014.

[14] A. Hadaeghi, H. Samet, and T. Ghanbari, "Multi SVR approach for fault location in multi-terminal HVDC systems," *International Journal of Renewable Energy Research (IJRER)*, Vol. 9, No. 1, pp. 194–206, Mar. 2019.

[15] S. Chaithanya, V. N. B. Reddy, and R. Kiranmayi, "A state of art review on offshore wind power transmission using low frequency AC system," *International Journal of Renewable Energy Research (IJRER)*, Vol. 8, No. 1, pp. 141–149, Mar. 2018.

[16] L. Hanqing, L. Yadong, S. Gehao, and J. Xiuchen, "Fault-cause identification method based on adaptive deep belief network and time–frequency characteristics of travelling wave," *IET Generation, Transmission & Distribution*, Vol. 13, No. 5, pp. 724–732, Mar. 2019.

[17] X. Feng, L. Qi, and J. Pan, "A novel location method and algorithm for DC distribution protection," *IEEE Transactions on Industry Applications*, Vol. 53, No. 3, pp. 1834–1840, 2017.

[18] A. Meghwani, S. C. Srivastava, and S. Chakrabarti, "Local measurement-based technique for estimating fault location in multi-source DC microgrids," *IET Generation, Transmission & Distribution*, Vol. 12, No. 13, pp. 3305–3313, 2018.

[19] B. Rathore and A. G. Shaik, "Wavelet-alienation based transmission line protection scheme," *IET Generation, Transmission & Distribution*, Vol. 11, No. 4, pp. 995–1003, 2017.

[20] J. Duan, K. Zhang, and L. Cheng, "Novel method of fault location for single phase microgrids," *IEEE Transactions on Smart Grid*, Vol. 7, No. 2, pp. 915–925, 2016.

[21] M. Monadi, C. Gavriluta, A. Luna, I. Candela, and P. Rodriguez, "Centralized protection strategy for medium voltage DC microgrids," *IEEE Transactions on Power Delivery*, Vol. 32, No. 1, pp. 430–440, Feb. 2017.

[22] S. Dhar, R. K. Patnaik, and P. K. Dash, "Fault detection and location of photovoltaic based DC microgrid using differential protection strategy," *IEEE Transactions on Smart Grid*, Vol. 9, No. 5, pp. 4303-4312, 2017.

[23] S. Fletcher, P. J. Norman, K. Fong, S. J. Galloway, and G. M. Burt, "High-speed differential protection for smart DC distribution systems," *IEEE Transactions on Smart Grid*, Vol. 5, No. 5, pp. 2610–2617, Sep. 2014.

[24] R. Mohanty and A. K. Pradhan, "DC ring bus microgrid protection using the oscillation frequency and transient power," *IEEE Systems Journal*, Vol. 13, No. 1, pp. 875–884, Mar. 2019.

[25] J. D. Park, J. Candelaria, L. Ma, and K. Dunn, "DC ring-bus microgrid fault protection and identification of fault location," *IEEE Transactions on Power Delivery*, Vol. 28, No. 4, pp. 2574–2584 2013.

[26] M. Anun, M. Ordonez, I. G. Zurbriggen, and G. G. Oggier, "Circular switching surface technique: High-performance constant power load stabilization for electric vehicle systems," *IEEE Transactions on Power Electronics*, Vol. 30, No. 8, pp. 4560–4572, Aug. 2015.

[27] E. Christopher, M. Sumner, D. W. Thomas, X. Wang, and F. de Wildt, "Fault location in a zonal DC marine power system using active impedance estimation," *IEEE Transactions on Industry Applications*, Vol. 49, No. 2, pp. 860–865, 2013.

[28] A. K. Pradhan and R. Mohanty, "Cable fault location in a DC microgrid using current injection technique," in *National Power Systems Conference (NPSC)*, pp. 1–6, Dec. 2016.

[29] M. M. Xu, L. Y. Xiao, and H. F. Wang, "A prony-based method of locating shortcircuit fault in DC distribution system," in *2nd IET Renewable Power Generation Conference*, Beijing, China, pp. 1–4, Sep. 2013.

[30] F. Paz and M. Ordonez, "High-performance solar MPPT using switching ripple identification based on a lock-in amplifier," *IEEE Transactions on Industrial Electronics*, Vol. 63, No. 6, pp. 3595–3604, Jun. 2016.

[31] R. Mohanty, U. S. M. Balaji, and A. K. Pradhan, "An accurate noniterative fault location technique for low-voltage DC microgrid," *IEEE Transactions on Power Delivery*, Vol. 31, No. 2, pp. 475–481, 2016.

[32] J. Park, "Ground fault detection and location for ungrounded DC traction power systems," *IEEE Transactions on Vehicular Technology*, Vol. 64, No. 12, pp. 5667–5676, 2015.

[33] K. Jia, T. Bi, B. Liu, E. Christopher, D. W. Thomas, and M. Sumner, "Marine power distribution system fault location using a portable injection unit," *IEEE Transactions on Power Delivery*, Vol. 30, No. 2, pp. 818–826, 2015.

[34] M. Zadsar, M. R. Haghifam, and S. M. M. Larimi, "Approach for self-healing resilient operation of active distribution network with microgrid," *IET Generation, Transmission & Distribution*, Vol. 11, No. 18, pp. 4633–4643, 2017.

[35] S. Gautam and S. M. Brahma, "Detection of high impedance fault in power distribution systems using mathematical morphology," *IEEE Transactions on Power Systems*, Vol. 28, No. 2, pp. 1226–1234, 2013.

[36] L. L. Zhang, M. S. Li, T. Y. Ji, Q. H. Wu, L. Jiang, and J. P. Zhan, "Morphology singular entropy-based phase selector using short data window for transmission lines," *IEEE Transactions on Power Delivery*, Vol. 26, No. 5, pp. 2162–2171, 2011.

[37] F. Namdari and M. Salehi, "A high-speed protection scheme based on initial current traveling wave for transmission lines employing mathematical morphology," *IEEE Transactions on Power Delivery*, Vol. 32, No. 1, pp. 246–253, 2017.

[38] S. Mallat, *A wavelet tour of signal processing*. Academic Press: California, 1999.

[39] S. M. Shahrtash and F. Haghjoo, "Reduced instant wavelet transform decomposition filter for on-line applications," *Submitted to Iranian Journal of Science and Technology*, 2008.

M. Dodangeh received the B.Sc. degree in Electrical Engineering from the University of Zanjan, Zanjan, Iran, in 2011, the M.Sc. degree in Electrical Engineering from Imam Khomeini International University, Qazvin, Iran, in 2015, and is currently pursuing the Ph.D. degree in Electrical Engineering at the Imam Khomeini International University, Qazvin, Iran. His research interests include power system studies, such as applications of digital signal processing in power system protection, micro grids, digital protective relays, power system stability, and power system optimization problems.

N. Ghaffarzadeh is an Associate Professor of Electrical Engineering at Imam Khomeini International University. His special fields of interest include power system protection and transient in power systems. He is the author of five books in the field of power systems. He is also the author and the coauthor of over 100 technical papers.